Spectral solution of load flow equations

J.-G. Caputo, A. Knippel and N. Retiere

August 22, 2018

1 Introduction

The electrical grid is one of the major engineering achievements of the 20th century. Originally designed to distribute electricity from large generators, it is changing rapidly due to the emergence of renewable and intermittent sources, energy storage and electric vehicles [2]. Not adressed properly, this complexity could result in management difficulties and possible black-outs. The main model used by operators and planners is the so-called load-flow equations[1] for stationary electrical networks, connecting incoming power to voltage and current. These equations are nonlinear and can only be solved numerically. They are used to reconfigure the network depending on the availability of power sources.

An important issue for the network is to predict the critical lines, i.e. the ones that are most heavily loaded. These have more losses and usually black outs start from them. These can be computed using the the load-flow equations but one cannot predict easily how they change depending on the distribution of generators and loads. Also the load-flow does not explain how they are affected by the topology of the network. A global geometrical point of view, incoporating the topology and the load-generator distribution would be very useful to address this issue. This is what we propose in this article. We reduce the load-flow equations to the DC load flow which is a Laplacian equation [6] and proceed to solve it using a spectral approach. This naturally shows the dependence of the critical lines on the topology and load-generator distribution. It is a Fourier like picture of the network useful for planning. It also allows for rapid adjustments of the network which are much faster than solving the load-flow equations. We obtain an explicit Parseval relation for the quadratic energy in the lines which can be used for minimization. Finally the evolution of L_2 and L_∞ partial sums as a function of i show that low order modes contribute most so that the full modal decomposition is not necessary. For example, for a

115 node network, 15 modes are sufficient to describe the solution with a 5 % accuracy.
The article is organized as follows. Section 2 recalls the load-flow equations and how they can be approximated by a Laplace equation. We introduce the spectral solution of this equation in section 3. Section 4 presents the spectrum of some IEEE networks and section 5 illustrates the spectral solution of the reduced load-flow. Conclusions are presented in section 6.

2 The load-flow equations

To derive these equations, we will follow the very clear derivation of [4]. At each node, we write conservation of power, this means

$$\mathcal{P} = \mathcal{V}\mathcal{I}^*, \tag{1}$$

where $\mathcal{P}$ is the vector of powers inserted into or extracted from the network, each component corresponding to a node. The right hand side is the power due to the network. From the generalization of Ohm's law

$$\mathcal{I} = (G + jB)(V + jW), \tag{2}$$

where $G + jB$ is the so-called $Ybus$ matrix [1]. We then get

$$\mathcal{I}^* = (GV - BW) + j(-BV - GW). \tag{3}$$

Combining (1) and (3), we obtain

$$\mathcal{P} = V(GV - BW) + W(BV + GW) + j[W(GV - BW) + V(-BV - GW)]. \tag{4}$$

Introducing the vector of active and reactive powers, so that

$$\mathcal{P} = P + jQ, \tag{5}$$

we obtain our final load flow equations [4]

$$V(GV - BW) + W(BV + GW) = P, \tag{6}$$

$$W(GV - BW) + V(-BV - GW) = Q. \tag{7}$$

In index notation, the system is written as

$$V_k \sum_i (G_{ki}V_i - B_{ki}W_i) + W_k \sum_i (B_{ki}V_k + G_{ki}W_i) = P_k, \tag{8}$$

$$W_k \sum_i (G_{ki}V_i - B_{ki}W_i) - V_k \sum_i (B_{ki}V_k + G_{ki}W_i) = Q_k. \tag{9}$$

The sums correspond to matrix-vector multiplications while the terms on the left of the sums correspond to tensor products. The two operations do not commute.
The system (6) is quadratic in V and W and needs to be solved using an optimization solver, for example a Newton-Raphson method. In the next section, we will simplify the system for a transmission network.

2.1 Simplified model of a transmission network

For such a network, three main assumptions can be made

- neglect the ohmic part of the $Ybus$ matrix so take $G = 0$
- assume that voltage modulus is constant
- assume that phase is small

Taking $G = 0$ leads to the new system

$$-V(BW) + W(BV) = P, \tag{10}$$
$$-W(BW) - V(BV) = Q. \tag{11}$$

The second assumption implies

$$\mathcal{V} = V + jW \equiv ve^{j\theta} \approx 1 + j\theta, \tag{12}$$

because the vector $v \approx 1$. Then the vectors V, W are

$$V = 1, \quad W = \theta.$$

The first equation of (10) reduces to

$$-B\theta = P. \tag{13}$$

This is a singular linear system to be solved for the vector of phases θ knowing the vector of active powers P. To identify critical links we compute the power line vector P_l whose components are the powers in each line. It is calculated using by the discrete gradient ∇ (see [5] for an example)

$$\nabla\theta = P_l. \tag{14}$$

The two equations (13-14) are the main model that we will consider in the rest of the article. Since the matrix B is a graph Laplacian, it is singular and the linear system (13) needs to be solved with care. In the next section, we will use the important symmetries of B to solve (13).

Note that a similar simplification of the load-flow equations can be done for distribution networks. For those networks, we can assume

$$B = 0, \quad W \approx 0, \quad V = 1 + \delta V$$

This leads to the following equation, very similar to (13)

$$P = G\delta V. \tag{15}$$

In the following we consider for simplicity that the discrete gradient ∇ and the Laplacian matrix B are normalized so that all their entries are integers. At line i the diagonal of the Laplacian is minus the degree of node i. The spectral formalism that we present below carries through entirely in the presence of weights.

3 Spectral solution of the reduced load-flow

In this section, we use the notation from graph theory and note the graph Laplacian matrix B, Δ. The matrix Δ is symmetric and positive. Its eigenvalues can be written

$$\omega_1^2 = 0 \leq \omega_2^2 \leq \cdots \leq \omega_n^2,$$

where n is the number of nodes of the network. The eigenvectors

$$v^1, v^2, \ldots v^n,$$

can be chosen orthogonal. In the rest of the article, we assume that the network is connected so that $\omega_1^2 = 0 < \omega_2^2$ [6].

A standard way of solving equation (13) is to use the Penrose pseudo-inverse with a regularization [7] to eliminate the zero eigenvalue. This does not give much information on the way the solution depends on the graph and the power distribution. To gain insight, it is useful to project P on these vectors

$$P = p_1 v^1 + p_2 v^2 + \cdots + p_n v^n, \tag{16}$$

and take advantage on the orthogonality of the eigenvectors. Assuming that the powers are balanced $p_1 = 0$, one can immediately calculate θ as

$$\theta = -\frac{p_2}{\omega_2^2} v^2 - \frac{p_3}{\omega_3^2} v^3 \cdots - \frac{p_n}{\omega_n^2} v^n. \tag{17}$$

The power in the lines P_l is then

$$P_l = \nabla\theta = -\frac{p_2}{\omega_2^2} \nabla v^2 - \frac{p_3}{\omega_3^2} \nabla v^3 \cdots - \frac{p_n}{\omega_n^2} \nabla v^n. \tag{18}$$

Let us now be specific about the distribution of generators and loads in the network. We introduce the vectors G and L and their components

$$P \equiv G - L, \quad G = \sum_{i=1}^{n} g_i v^i, \quad L = \sum_{i=1}^{n} l_i v^i. \tag{19}$$

First note that

$$\sum_{k=1}^{n} P_k = \sum_{k=1}^{n} (G_k - L_k) = \sum_{i=1}^{n} (g_i - l_i)(\sum_{k=1}^{n} v_k^i) = \frac{g_1 - l_1}{\sqrt{n}} = 0,$$

because $\sum_{k=1}^{n} v_k^i = 0, i > 1$ and the network is balanced ($g_1 = l_1$). The euclidian norm of P_l has a particularly simple form. To see this we write

$$\| P_l \|_2^2 = \sum_{i,j=2}^{n} \frac{(g_i - l_i)(g_j - l_j)}{\omega_i^2 \omega_j^2} (\nabla v^i)^T \nabla v^j.$$

Note that

$$(\nabla v^i)^T \nabla v^j = (v^i)^T (\nabla^T \nabla) v^j = (v^i)^T \Delta v^j = \omega_i^2 \delta_{ij},$$

where δ_{ij} is the Kronecker symbol. We get finally the Parseval like relation

$$\| P_l \|_2^2 = \sum_{i=2}^{n} \frac{(g_i - l_i)^2}{\omega_i^2}. \tag{20}$$

The L_2 norm of the power is this simple expression depending only on the eigenvalues and the projections of the input-output powers on the eigenvectors. In the following we will use this expression to guide the changes to the generator or load distributions.
Expression (20) also holds for the weighted Laplacian, so that (20) can be used for real electrical networks.

3.1 Theoretical background : nodal domains

The vectors ∇v^i give rise to the so-called nodal domains. We recall the following definitions and theorem following the presentation of [9].

Definition 3.1 (Nodal domain) *A positive (negative) nodal domain of a function f defined on the vertices of a graph $G(V, E)$ is a maximal connected induced subgraph of G on vertices $v \in V$ with $f(v) \geq 0$ ($f(v) \leq 0$).*

For a strong positive nodal domain, the sign $\geq$ should be replaced by $>$. In the electrical grid context, positive nodal domains correspond to generators while negative nodal domains are loads.

We call $\mathcal{S}(f), \mathcal{W}(f)$, respectively the positive strong and weak nodal domains of a eigenfunction f. We have the following result [10].

Theorem 3.2 (Discrete nodal domain theorem) *Let Δ be a generalized Laplacian of a connected graph with n vertices. Then, any eigenfunction f_k corresponding to the kth eigenvalue λ_k with multiplicity r has at most k weak nodal domains and $k + r - 1$ strong nodal domains.*
$\mathcal{S}(f_k) \leq k, \qquad \mathcal{W}(f_k) \leq k + r - 1.$

Then, the nodal domains are small (resp. large) scale for large (resp. small) i. In particular, the first non zero eigenvalue partitions the graph, see the following result from Fiedler [8].

Theorem 3.3 *An eigenfunction of second eigenvalue has exactly two nodal domains.*

3.2 Decay of inverse of eigenvalues

Let us comment on the behavior of the eigenvalues $-\omega_i^2$ of the graph Laplacian as a function of i. The following bounds are known [6]

$$\frac{n-1}{n}\omega_2^2 \leq \bar{d} \leq \frac{n-1}{n}\omega_n^2$$

where $\bar{d} = 2m/n$ is the average degree and m is the number of links. Using the definition of $\bar{d}$ we reduce this to

$$\frac{1}{\omega_2^2} \geq \frac{n-1}{2m}, \qquad \frac{1}{\omega_n^2} \leq \frac{n-1}{2m}. \tag{21}$$

For complete graphs, $m = n(n-1)/2$ so that $\omega_n^2 \geq n$. This bound is sharp because complete graphs have $n-2$ eigenvalues equal to n. Electrical networks are far from complete graphs so that we expect the average degree $2 \leq \bar{d} \leq 3$. Then the eigenvalues increase slowly with n.

3.3 Practical consequences for electrical networks

The spectral approach that we present gives a geometric picture of the network and the power vector. It gives a quick approximation of the solution of the nonlinear load-flow equations.

Relation (20) gives explicitly the L_2 norm of the energy in the lines. This remarkable result provides a way to optimize the electrical network. If the infinite norm is required, then we just use formula (18). The following bounds for the L_∞ norm can be used

$$\frac{\| P_l \|_2}{n} \leq \| P_l \|_\infty \leq \| P_l \|_2 . \tag{22}$$

The relation (20) implies that taking $g_i = l_i$ makes the power in all the lines zero. This corresponds to not having any network. Each node has a generator exactly balancing its load. This is of course not reasonable. Instead (20) seems to indicate that the dominating terms are the small $i = 2, 3, 4..$ terms. Then, to minimize the expression we can choose the corresponding amplitudes $g_i - l_i$ to be small. This naive analysis will be checked carefully and confirmed below.

4 Spectral features of some IEEE networks

4.1 IEEE Case 30

As an example, we use the case30 from IEEE. Fig. 1 shows the network of $n = 30$ nodes, $m = 41$ edges and $\bar{d} = 2m/n \approx 2.7$.

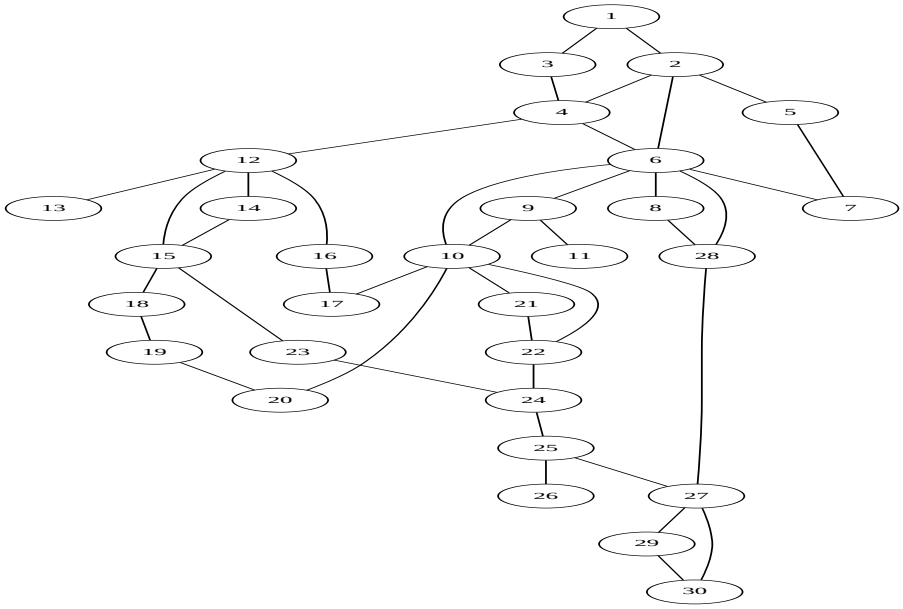

Figure 1: Schematic of the IEEE network case 30, from [12] using the Graphviz software [11].

We take the same weights on each branch. For each index i, we compute the inverse of the eigenvalue $1/\omega_i^2$; it decays as a function of i as shown in the left panel of Fig. 2. We scale the eigenvectors v^i so that the sum of the positive components is equal to 1, this corresponds to having an equal input power in the network independently of i. The norm of $\| \nabla v^i \|_\infty$ increases with i and has some maxima. It is shown in the right panel of Fig. 2.

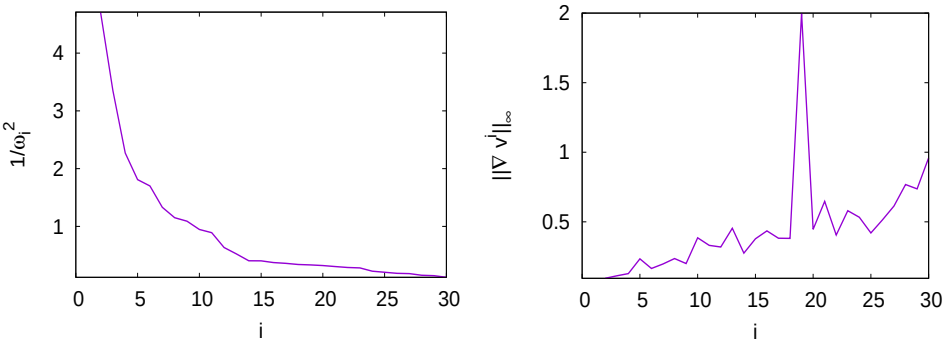

Figure 2: Plot as a function of i of the inverse of the eigenvalue $1/\omega_i^2$ (left panel) and of $\| \nabla v^i \|_\infty$ (right panel) .

The associated line power infinite norm $\| P_l \|_\infty$ which is the multiplication of the two different expressions is shown in Fig. 3.

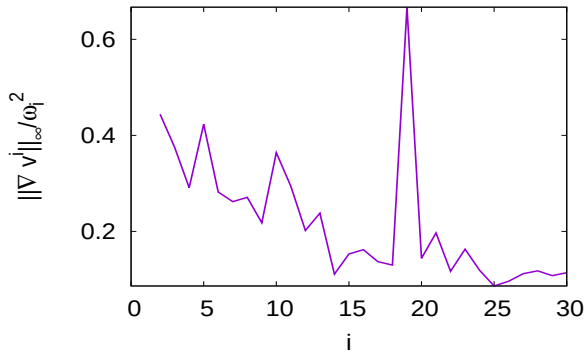

Figure 3: Plot of the line power infinite norm $\| P_l \|_\infty$ when $P = v^i$ as a function of i.

Note the peak for $i = 19$ which corresponds to the swivel eigenvector v^{19} such that $v^{19}_{29} = +1/\sqrt{2}$, $v^{19}_{30} = -1/\sqrt{2}$, $v^{19}_i = 0$ for i different from $29, 30$. The nodes 29 and 30 correspond to a swivel [5] so that all the other nodes are zero or "soft" in our terminology. The eigenvalue is $-\omega^2_{19} = -1$. This swivel eigenvector is the one giving the maximum $\| P_l \|_\infty$. The other eigenvectors that give peaks in $\| P_l \|_\infty$ are v^5 and v^{10}. Their nodal domains are much more complex than the one of v^{19} and are shown in Figs. 4 and 5.

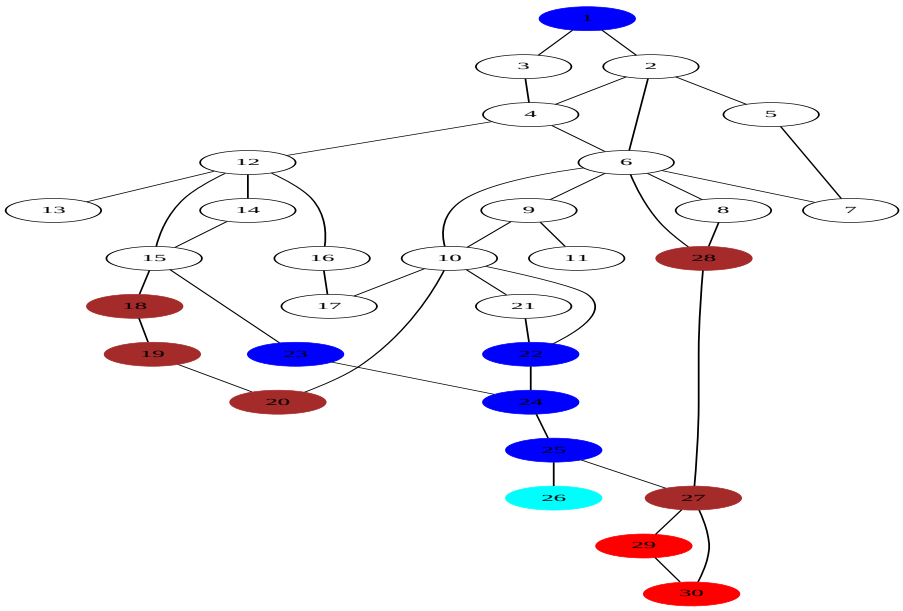

Figure 4: Nodal domains of the eigenvector v^5. The color scheme is red $[-0.5 - 0.3]$, brown $[-0.3 - 0.1]$ black $[-0.10.1]$, cyan $[0.10.3]$ and blue $[0.30.5]$.

Notice the strong gradient around nodes 25,26 and 27.

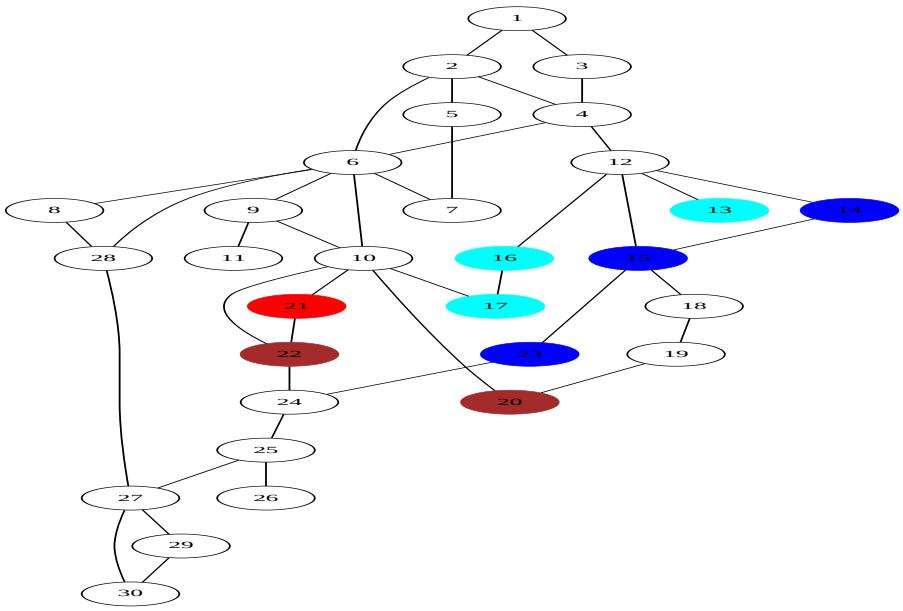

Figure 5: Nodal domains of the eigenvector v^{10}, the color scheme is the same as for Fig. 4 .

Notice the strong gradient around nodes 10, 21 and 17.

4.2 IEEE Case 118

The next example is the larger case118 with $n = 118$ nodes, $m = 186$ edges and an average degree $\bar{d} = 2m/n = 3.1$. Again we take the same weights on the branches. The results are shown in Figs. 6 and 7. They are very similar to the ones for the case30. In particular, the inverse of the eigenvalues decay exponentially as shown in the log-log scale of the left panel of Fig. 6.

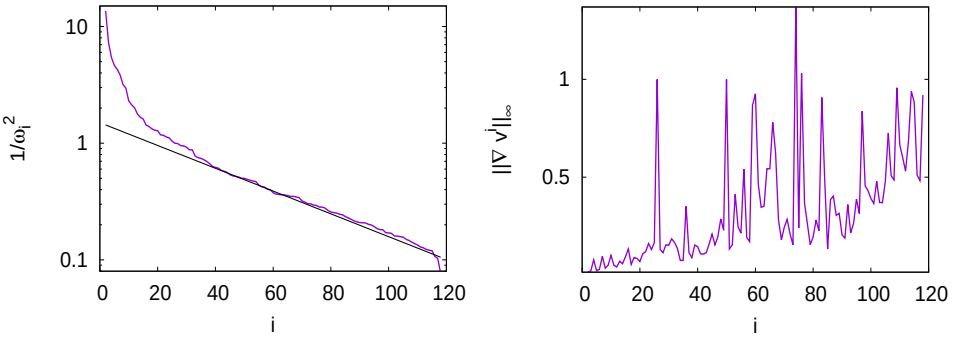

Figure 6: Plot as a function of i of the inverse of the eigenvalue $1/\omega_i^2$ (left panel) and of $\| \nabla v^i \|_\infty$ (right panel) .

The associated line power infinite norm $\| P_l \|_\infty$ is shown in Fig. 7. As for case 30, the peak for $i = 26$ corresponds to the swivel eigenvector [5] v^{26} such that $v^{26}_{111} = +1/\sqrt{2}$, $v^{26}_{112} = -1/\sqrt{2}$, $v^{26}_i = 0$ for i different from 111, 112. The eigenvalue is $-\omega^2_{26} = -1$.

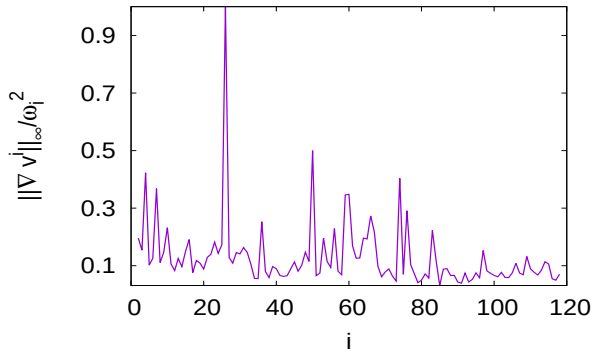

Figure 7: Plot of the line power infinite norm $\| P_l \|_\infty$ when $P = v^i$ as a function of i.

5 Spectral solutions of the reduced load-flow

5.1 A small size network : effect of soft nodes

Before addressing networks with a relatively large number of nodes it is useful to consider a very simple example where calculations can be conducted by hand.

This show the usefulness of the approach.

We consider the simple 6 node network shown in Fig. 8.

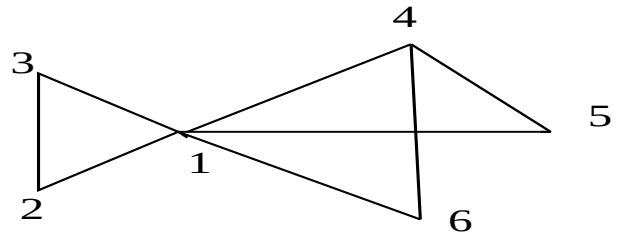

Figure 8: A 6-node electrical network.

The graph Laplacian here is

$$\Delta = \begin{pmatrix} 5 & -1 & -1 & -1 & -1 & -1 \\ -1 & 2 & -1 & 0 & 0 & 0 \\ -1 & -1 & 2 & 0 & 0 & 0 \\ -1 & 0 & 0 & 3 & -1 & -1 \\ -1 & 0 & 0 & -1 & 2 & 0 \\ -1 & 0 & 0 & -1 & 0 & 2 \end{pmatrix}, \tag{23}$$

whose eigenvalues are

$$\omega_1^2 = 0,\ \omega_2^2 = 1,\ \omega_3^2 = 2,\ \omega_4^2 = 3,\ \omega_5^2 = 4,\ \omega_6^2 = 6 \tag{24}$$

corresponding to the eigenvectors matrix

$$\begin{aligned} v^1 &= \frac{1}{\sqrt{6}}(1,1,1,1,1,1)^T, \quad v^2 = \frac{1}{\sqrt{30}}(0,3,3,-2,-2,-2)^T, \\ v^3 &= \frac{1}{\sqrt{2}}(0,0,0,0,1,-1)^T, \quad v^4 = \frac{1}{\sqrt{2}}(0,1,-1,0,0,0)^T, \\ v^5 &= \frac{1}{\sqrt{6}}(0,0,0,2,-1,-1)^T, \quad v^6 = \frac{1}{\sqrt{30}}(-5,1,1,1,1,1)^T,. \end{aligned}$$

The associated gradients are

$$\begin{aligned} &\nabla v^2 \approx (-0.55,0,0.55,0.36,0,-0.36,0.36,0)^T, \quad \nabla v^3 \approx (0,0,0,0,-0.71,0.71,0.71,0.71)^T, \\ &\nabla v^4 \approx (0.71,-1.41,0.71,0,0,0,0,0)^T, \quad \nabla v^5 \approx (0,0,0,0.82,-1.22,0.41,-0.41,-1.22)^T, \\ &\nabla v^6 \approx (-1.09,0,1.09,-1.09,0,1.09,-1.09,0)^T. \end{aligned} \tag{25}$$

The power in the lines is then

$$P_l = p_2\frac{\nabla v^2}{1} + p_3\frac{\nabla v^3}{2} + p_4\frac{\nabla v^4}{3} + p_5\frac{\nabla v^5}{4} + p_6\frac{\nabla v^6}{6}, \tag{26}$$

where p_i is the projection of P on the eigenvector v^i, see (16). From this, it is clear that a large p_2 will contribute significantly more to P_l than a large p_5 or p_6. When the eigenvector v^i has a zero component at node k (a soft node in the language i of [5]), the p_i coefficient is not influenced by what is at node k. In particular, if there is a generator there, it will not influence p_i.

To see these effects in more detail, we first assume that the loads are equally distributed over the network and study how placing a single generator on the network affects P_l. To examine the contribution of the different modes v^i to P_l, we introduce the partial sums

$$s_k^\infty = \| \sum_{i=1}^{k} (g_i - l_i) \frac{\nabla v^i}{\omega_i^2} \|_\infty, \tag{27}$$

$$s_k^2 = \sum_{i=1}^{k} \frac{(g_i - l_i)^2}{\omega_i^2}. \tag{28}$$

Note that $s_n^2 = \| P_l \|_2^2$ and $s_n^\infty = \| P_l \|_\infty$.

position of generator	1	2	4	6
p_2	0	-3.29	2.19	2.19
p_3	0	0	0	-4.24
p_4	0	4.24	0	0
p_5	0	0	5	-2.44
p_6	5.48	-1.09	-1.09	-1.09
$\| P_l \|_\infty$	1	3	2	2.75
$\| P_l \|_2$	2.24	4.12	3.32	3.94

Table 1: Power coefficients p_i, $\| P_l \|_\infty$, $\| P_l \|_2$ and partial sums s_k^∞ and s_k^2 for different generator positions. The loads are uniform.

Table 1 shows the coefficients p_i for a generator of strength 6 placed at nodes 1, 2 or 4. A generator at node 1 will be such that only p_6 is non zero. Then we expect that $\| P_l \|$ will be minimal and this is indeed the case. On the other hand, a generator placed at node 2 gives a large p_2 so that $\| P_l \|$ will be larger. As expected, we see in table 1 a correlation between large values of p_2 and p_3 and large values of $\| P_l \|$.

In a second set of experiments, we place two generators on the grid and examine how P_l depends on their position. For this, we choose the following vector of loads

$$L = (1, 2, 1, 3, 0, 1)^T.$$

First we assume that the generators are placed at nodes 1 and 2. The power vector is $P = (g - 1, 6 - g, -1, -3, 0, -1)^T$. Projecting P onto the eigenvectors,

we note that, because of the zero components v_1^3 and v_1^5, there are no g dependent components on the eigenvectors v^3 and v^5; we find $\parallel P_l \parallel_2 = 2.7$. When the generators are now placed at nodes 1 and 5, g terms will affect the components of v^2, v^3, v^5 and v^6. We then expect to find a higher maximum for $\parallel P_l \parallel_2$ and this is the case, $\parallel P_l \parallel_2 = 3.2$. Fig. 9 shows $\parallel P_l \parallel_2$ (blue online) and $\parallel P_l \parallel_\infty$ (red online) as a function of g for the two different configurations. We see that $\parallel P_l \parallel_2$ for the 1-2 configuration (left) is always above $\parallel P_l \parallel_2$ for the 1-5 configuration (right). On the other hand, the minimum of $\parallel P_l \parallel_\infty$ is the same for both configurations.

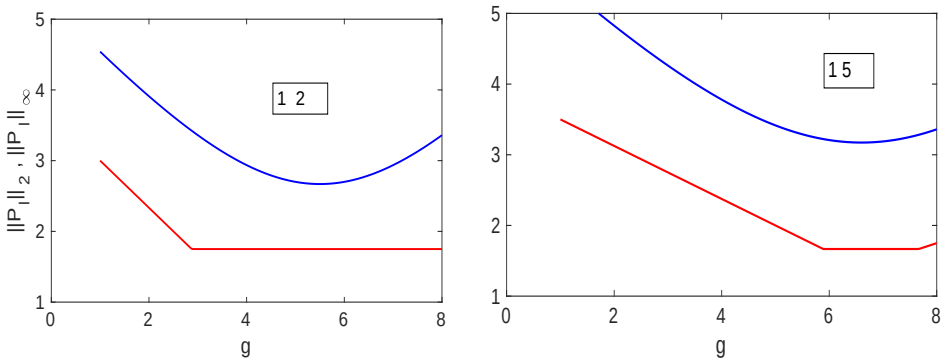

Figure 9: Plot of $\parallel P_l \parallel_2$ (blue online) and $\parallel P_l \parallel_\infty$ (red online) as a function of the strength g of the generator at node 1, when the second generator is placed at node 2 (left panel) or at node 5 (right panel).

The flatness of $\parallel P_l \parallel_\infty$ for the 1-2 distribution (left of Fig. 9) is due to the zero first and second components for v^i. On the other hand the 1-5 distribution has less zeros so the $\parallel P_l \parallel_\infty$ depends more on g.

We now place the 1st generator of amplitude g at node 2 and the second one at nodes 4,5 and 6 respectively. Fig. 10 shows $\parallel P_l \parallel_2 \parallel P_l \parallel_2$ (blue online) and $\parallel P_l \parallel_\infty$ (red online) as a function of g.

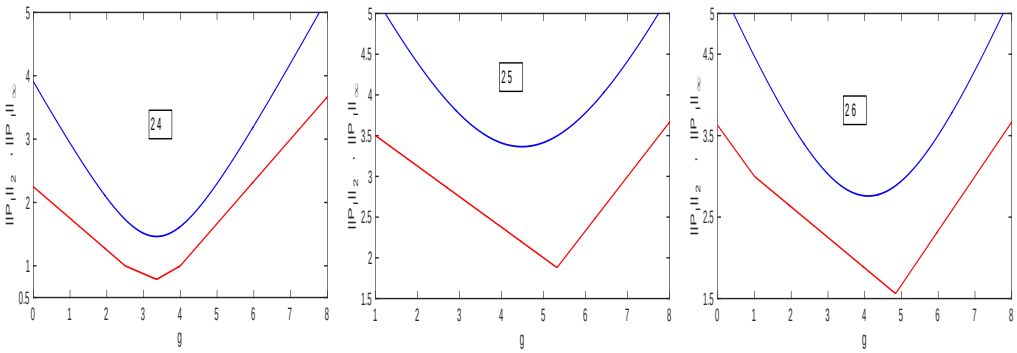

Figure 10: Plot of $\| P_l \|_2$ (blue online) and $\| P_l \|_\infty$ (red online) as a function of the strength g of the generator at node 2, when the second generator is placed at nodes 4,5 and 6.

We see that the 2-4 configuration gives a minimum compared to the 2-5 and 2-6. This is clear because in this configuration, the v^3 component of P does not depend on g.

5.2 Evolution of partial sums: example of a cartesian grid

For the placement of two generators on a network, it is interesting to write $\| P_l \|_2^2$. Assuming the generators are positioned at nodes k and m , with amplitudes G_k and G_m, we have

$$\| P_l \|_2^2 = \sum_{i=2}^{n} \frac{(g_i - l_i)^2}{\omega_i^2} = \sum_{i=2}^{n} \frac{(G_k v_k^i + G_m v_m^i - l_i)^2}{\omega_i^2}.$$

Expanding the squares and rearranging, we get the final expression

$$\| P_l \|_2^2 = G_k^2 \sum_i \frac{(v_k^i)^2}{\omega_i^2} + G_m^2 \sum_i \frac{(v_m^i)^2}{\omega_i^2}$$

$$+ \sum_i \frac{(l_i)^2}{\omega_i^2} + 2G_k G_m \sum_i \frac{v_k^i v_m^i}{\omega_i^2} - 2G_k \sum_i \frac{v_k^i l_i}{\omega_i^2} - 2G_m \sum_i \frac{v_m^i l_i}{\omega_i^2}. \qquad (29)$$

The coefficients of this polynomial in G_k, G_m are sums from $i = 2$ to n. We have observed that they converge rapidly with i.

A simple system on which to test this convergence is a grid, i.e. the cartesian product of two chains. There, one can compute explicitly the eigenvectors and eigenvalues so that the network can be made arbitrarily large. A grid is also a first approximation of a transmission network.

Consider two chains C_n and C_m with n and m nodes respectively. The cartesian product $C_n \times C_m$ is the grid $n \times m$. Its eigenvalues are $\omega^2_{i,j} = \omega^2_i + \omega^2_j$ where ω^2_i is an eigenvalue for C_n while ω^2_j is an eigenvalue for C_m. The associated eigenvector is $v^{ij} = v^i \otimes v^j$, the Kronecker product of v^i and v^j. More details can be found in the book [9]. The eigenvalue $\omega^2_{i,j}$ and the components v^{ij}_{pq} are

$$\omega^2_{i,j} = 4\left[\sin^2\frac{\pi(i-1)}{2n} + \sin^2\frac{\pi(j-1)}{2m}\right], \tag{30}$$

$$v^{ij}_{pq} = v^i_p v^j_q = \frac{1}{N_p N_q}\cos[\frac{\pi(i-1)}{n}(p-\frac{1}{2})]\cos[\frac{\pi(j-1)}{m}(q-\frac{1}{2})], \tag{31}$$

where $i, p \in \{1, \ldots, n\}$, $\quad j, q \in \{1, \ldots, m\}$ and where the normalization factors are $N_p = \sqrt{n}$ if $p = 1$, $N_p = \sqrt{n/2}$ otherwise and $N_q = \sqrt{m}$ if $q = 1$ and $N_q = \sqrt{m/2}$ otherwise.

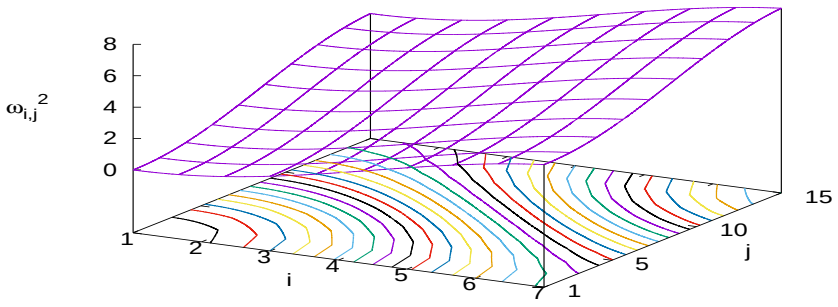

Figure 11: Eigenvalues $\omega^2_{i,j}$ as a function of i, j for a grid $n = 7, m = 15$. The contour lines are separated by 0.25.

The eigenvalues $\omega^2_{i,j}$ are such that $\omega^2_{i,j} \leq 8$. They increase monotonically with i and j as shown in Fig. 11; there the contour lines are separated by 0.25. To test the convergence of the sums leading to the coefficients G_k, G_m in (29), we introduce a cut-off index $n_s \leq n$ for the sums. We considered a grid of size $n = 61, m = 61$ and estimated how

$$\sum_{ij}^{n_s} \frac{v^{ij}_{pq} v^{ij}_{pq}}{\omega^2_{i,j}},$$

depends on n_s for $(p, q, r, s) = (10, 4, 20, 28), (10, 4, 10, 28), (4, 4, 6, 6)$ and $(4, 4, 15, 15)$. The results are shown in Fig. 12.

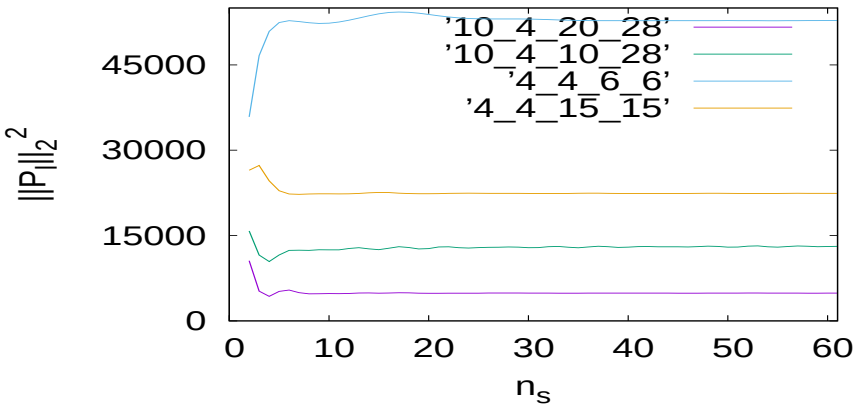

Figure 12: Partial sums $\sum_{ij}^{n_s} \frac{v_{pq}^{ij} v_{pq}^{ij}}{\omega_{i,j}^2}$, as function of n_s for different (p,q,r,s) configurations.

In all cases, except for the close nodes configuration $(4,4,6,6)$, the sum converges for $n_s \approx 10$. For the $(4,4,6,6)$ the sum has converged for $n_s \approx 20 \ll n$. The terms involving the loads l_i in (29) depend on the distribution of the loads. However for homogeneous loads, they can be computed. Then $l_i = 1, \forall i$ so that the sum can be computed assuming $r = s = 1$. The results are reported in Fig. 13 for $(p,q) = (4,4)$ and $(15,15)$ and again we observe convergence for $n_s \approx 10$ and $n_s \approx 20$.

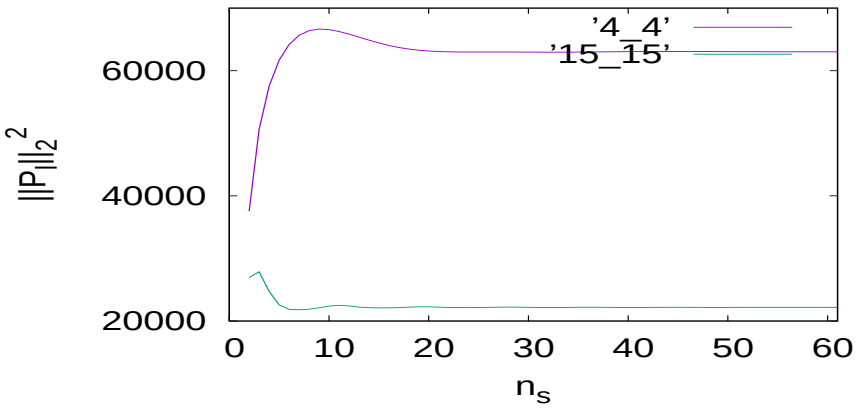

Figure 13: Partial sums $\sum_{ij}^{n_s} \frac{v_{pq}^{ij}}{\omega_{i,j}^2}$, as function of n_s for different (p,q) configurations.

5.3 The IEEE 30 network

There are only six generators in this network,

$$G_1 = 23.54,\ G_2 = 60.97,\ G_{13} = 37,\ G_{22} = 21.59,\ G_{23} = 19.2,\ G_{27} = 26.91. \tag{32}$$

The loads are distributed over the network.

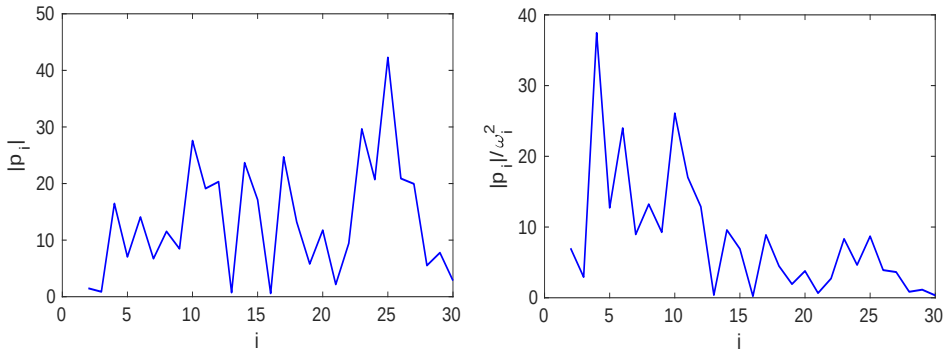

Figure 14: Plot of $|p_i|$ (left) and $\frac{|p_i|}{\omega_i^2}$ (right) as a function of i for the power vector P of IEEE case 30.

The components of the power vector P are shown in Fig. 14. As can be seen, they are about equally distributed.

First, we examine the convergence of s_k^∞, s_k^2 as k increases. The graph is shown in Fig. 15.

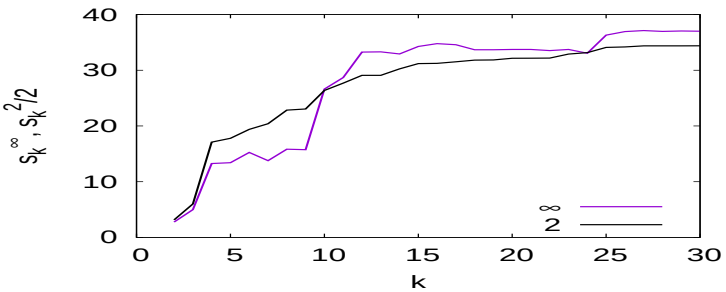

Figure 15: Plot of the partial sums s_k^∞, $s_k^2/2$ from (27,28) as a function of k.

Note how s_k^∞ and s_k^2 increase fast up to $k = 15$ terms. After that the rate of increase is much smaller. As expected, the small k eigenvalues dominate

the sum. Past $k = 12$, the L_∞ norm is stable while the L_2 norm continues to increase but at much slower rate.

We did not carry out a full optimization of the amplitudes of the generators since this is out of the scope of the article. Instead we varied the amplitudes G_i for to examine how the power in the lines varies. We show two cases in the table below

	G_1	G_2	G_{13}	G_{22}	G_{23}	G_{27}	$\| P_l \|_2$	$\| P_l \|_\infty$
original	23.54	60.97	37	21.59	19.2	26.91	68.78	37.
case 2			17		29.2	36.91	63.26	21.07

Table 2: Two different configurations of generators for IEEE case 30 with their associated line powers $\| P_l \|_2$ and $\| P_l \|_\infty$. Only the terms that have changed from the original configuration are reported.

We computed the partial sum s_k^∞ as a function of k for the four different configurations of table 2 in Fig. 16.

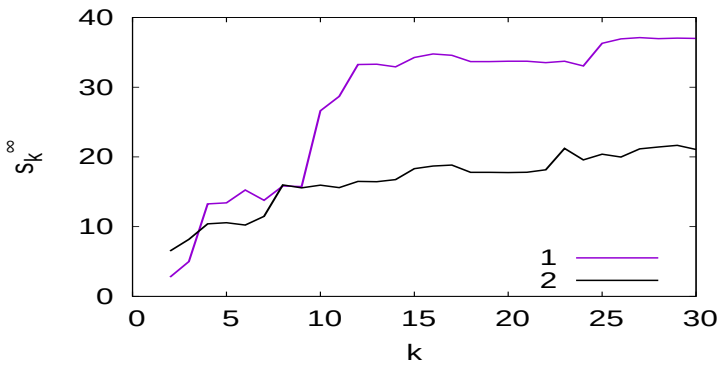

Figure 16: Plot of the partial sum (27) as a function of n for the two configurations shown in table 2

The configuration 2 has a much lower value of s_k^∞ than the other configuration. To show the importance of the modal distribution of power, we plot in Fig. 17 $|p_i|$ as a function of i for the two configurations.

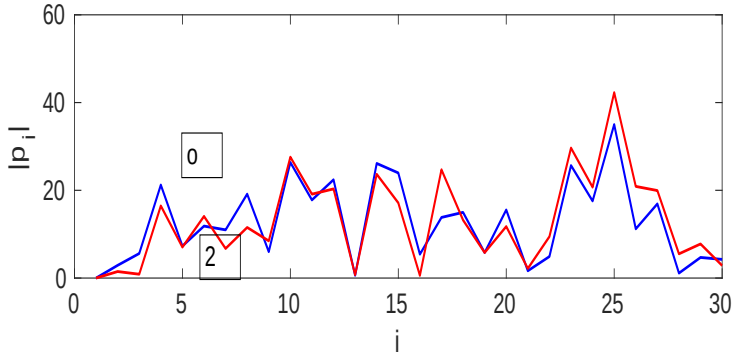

Figure 17: Plot of $|p_i|$ for the two configurations shown in table 2.

Indeed, we see that configuration 2 has smaller $|p_i|$ for $i < 15$ than the original configuration. This explains the difference in $\| P_l \|_2$ and especially $\| P_l \|_\infty$. This experiment shows that by tuning the amplitude of existing generators one can decrease significantly the power in the lines. We will carry out such an optimization in a further study.

5.4 The IEEE 118 network

The components of the power vector are shown in Fig. 18.

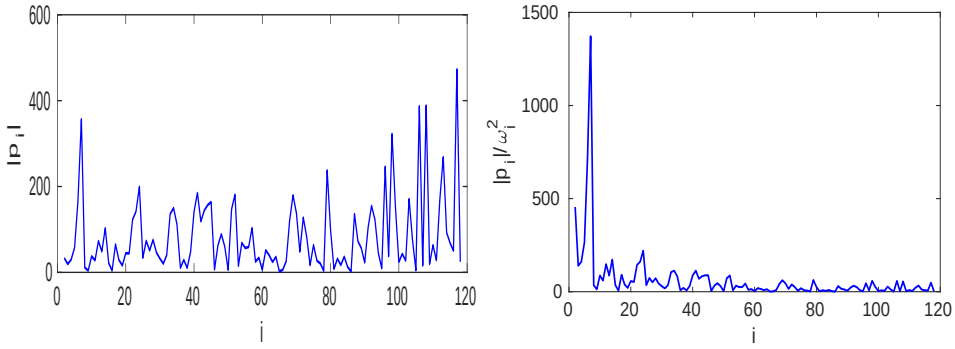

Figure 18: Plot of $|p_i|$ (left) and $\frac{|p_i|}{\omega_i^2}$ (right) as a function of i for the power vector P of IEEE case 118.

We examine the convergence of s_k^∞, s_k^2 as k increases. The graph is shown in Fig. 19.

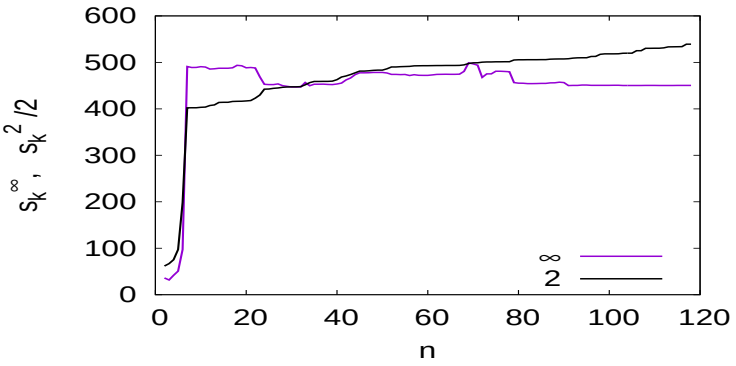

Figure 19: Plot of the partial sums s_k^∞ $s_k^2/2$ from (27,28) as a function of k.

As for case 30, both s_k^∞ and s_k^2 stabilize after 10 to 15 terms and again the small k eigenvalues dominate the sum.

6 Conclusion and discussion

We have shown that the load-flow equations can be reduced to a linear system involving the graph Laplacian. This system can be solved using a Fourier-like expansion of the power vector in the eigenvectors of the Laplacian.

This solution provides an explicit expression of $\| P_l \|_2$ in terms of eigenvalues ω_i^2 of the Laplacian. It shows the importance of soft nodes, where the eigenvectors have zero components. It also reveals that the main contribution to $\| P_l \|_2$ and especially to $\| P_l \|_\infty$ comes from the small i eigenvalues and eigenvectors. For example, only 10 or 20 modes are necessary to get a good estimate for a grid network of 360 nodes.

This geometric approach enables to plan electrical networks more efficiently than the standard nonlinear load-flow. It gives a global view of the network and the power vector. Because of this, in view of the growing portion of intermittent sources, our spectral approach allows to optimize and reconfigure networks rapidly. In the next paragraph, we illustrate some strategies that stem from our approach.

Some devices can work as generators and loads when they store the energy from the network. It is then important to distribute these special devices in a proper fashion to minimize $\| P_l \|_2$ and $\| P_l \|_\infty$. A natural way to do this is to preserve the spectral distribution of the power vector. A simple way to do this is to place storage close to the generators. When some production is lost, it is important to shed loads in a way that minimizes $\| P_l \|_\infty$. Again, the guideline

is to preserve the spectral content of the power vector. This will indicate which loads are better to shed.

Acknowledgements

The authors are funded by Agence Nationale de la Recherche grant "Fractal grid". The calculations were done at the CRIANN computing center.

References

[1] P. Kundur, "Power System Stability and Control" , Mac Graw-Hill, (1994).

[2] S. Backhaus and M. Chertkov, "Getting a grip on the electrical grid", Physics today 66 (5), 42 (2013).

[3] A. Grover-Silva, R. Girard and G. Kariniotakis, "Optimal sizing and placement of distribution grid connected battery systems through an SOCP optimal power flow algorithm", Applied energy, Elsevier (2017).

[4] D. K. Molzahn, C. Josz, I. A. Hiskens and P. Panciatici, arxiv.1507.07212

[5] J.G. Caputo, A. Knippel and E. Simo, J. Phys. A: Math. Theor. 46, 035100, (2013).

[6] D. Cvetkovic, P. Rowlinson and S. Simic, "An Introduction to the Theory of Graph Spectra", London Mathematical Society Student Texts (No. 75), (2001).

[7] W. H. Press , S. A. Teukolsky , W. T. Vetterling , B. P. Flannery , "Numerical Recipes: The Art of Scientific Computing", Cambridge University Press, (1986).

[8] M. Fiedler, Algebraic connectivity of graphs, Czechoslovak Math. J., 23(98) (1973), 298-305.

[9] T. Biyikoglu, J. Leydold and P. Stadler, "Laplacian eigenvectors of graphs", Springer (2000).

[10] E. B. Davies, G. M. L. Gladwell, J; Leydold and P. F. Stadler, "Discrete nodal domain theorems", Linear Algebra and its Applications 336 (2001) 51-60 .

[11] https://www.graphviz.org/

[12] https://www2.ee.washington.edu/research/pstca/pf30/pg_tca30bus.htm